J. Space Weather Space Clim. 2018, 8, A16

https://doi.org/10.1051/swsc/2018002

SWSC

Available online at:
www.swsc-journal.org

RESEARCH ARTICLE OPEN ACCESS

A new electron density model of the plasmasphere for operational applications and services

Norbert Jakowski* and Mohammed Mainul Hoque

German Aerospace Center, Institute of Communications and Navigation, Neustrelitz, Germany

Received 8 August 2017 / Accepted 10 January 2018

Abstract – The Earth's plasmasphere contributes essentially to total electron content (TEC) measurements from ground or satellite platforms. Furthermore, as an integral part of space weather, associated plasmaspheric phenomena must be addressed in conjunction with ionosphere weather monitoring by operational space weather services. For supporting space weather services and mitigation of propagation errors in Global Navigation Satellite Systems (GNSS) applications we have developed the empirical Neustrelitz plasmasphere model (NPSM). The model consists of an upper L shell dependent part and a lower altitude dependent part, both described by specific exponential decays. Here the McIllwain parameter L defines the geomagnetic field lines in a centered dipole model for the geomagnetic field. The coefficients of the developed approaches are successfully fitted to numerous electron density data derived from dual frequency GPS measurements on-board the CHAMP satellite mission from 2000 to 2005. The data are utilized for fitting up to the L shell $L = 3$ because a previous validation has shown a good agreement with IMAGE/RPI measurements up to this value. Using the solar radio flux index F10.7 as the only external parameter, the operation of the model is robust, with 40 coefficients fast and sufficiently accurate to be used as a background model for estimating TEC or electron density profiles in near real time GNSS applications and services. In addition to this, the model approach is sensitive to ionospheric coupling resulting in anomalies such as the Nighttime Winter Anomaly and the related Mid-Summer Nighttime Anomaly and even shows a slight plasmasphere compression of the dayside plasmasphere due to solar wind pressure. Modelled electron density and TEC values agree with estimates reported in the literature in similar cases.

Keywords: plasmasphere / empirical model / ionosphere / electron density / TEC

1 Introduction

After developing a series of empirical models which describe the temporal and spatial structure of key observables of the ionosphere/plasmasphere systems such as the total electron content (TEC), the ionospheric peak electron density NmF2 and its peak height hmF2 (Jakowski et al., 2011a; Hoque & Jakowski, 2011; 2012) we have developed an empirical model of the electron density distribution in the plasmasphere. The plasmasphere is the upward extension of the ionosphere co-rotating with the Earth up to the plasmapause height at about 3–5 Earth radii R_E (e.g. Lemaire & Gringauz, 1998; Darrouzet et al., 2009). Since the plasma consists mainly of cool H^+ ions and electrons in the region above the transition height at around 1000 km where the number of oxygen ions equalizes the number of protons, this region is also called protonosphere. The plasmasphere is an integral part of the Earth's space weather system and reacts very sensitive to solar storms via close coupling with the magnetosphere and ionosphere (e.g. Lemaire & Gringauz, 1998; Förster & Jakowski, 1988, 2000; Jakowski et al., 2007). Hence, to fully understand the behaviour of the geo-plasma under different solar and geophysical conditions, the plasmasphere is a challenging research target that has been addressed by many researchers over the last decades. Besides the development of a variety of remote sensing methods, considerable progress has been achieved in theoretical and empirical modelling (e.g. Gallagher et al., 1988; Lunt et al., 1999b; Webb & Essex, 2004; Huang et al., 2004; Pierrard et al., 2009; Reinisch et al., 2009; Pierrard & Voiculescu, 2011) to better understand internal plasma processes as well as coupling processes with the magnetosphere and ionosphere. Nevertheless, there remain many open questions concerning in particular plasma interaction with the magnetosphere, the formation of the plasmapause and coupling processes with the ionosphere in particular during space weather events. To better understand plasmaspheric dynamics, e.g. depletion and subsequent refilling of the plasmasphere in the course of geomagnetic storms lasting several days (e.g. Kersley &

*Corresponding author: norbert.jakowski@dlr.de

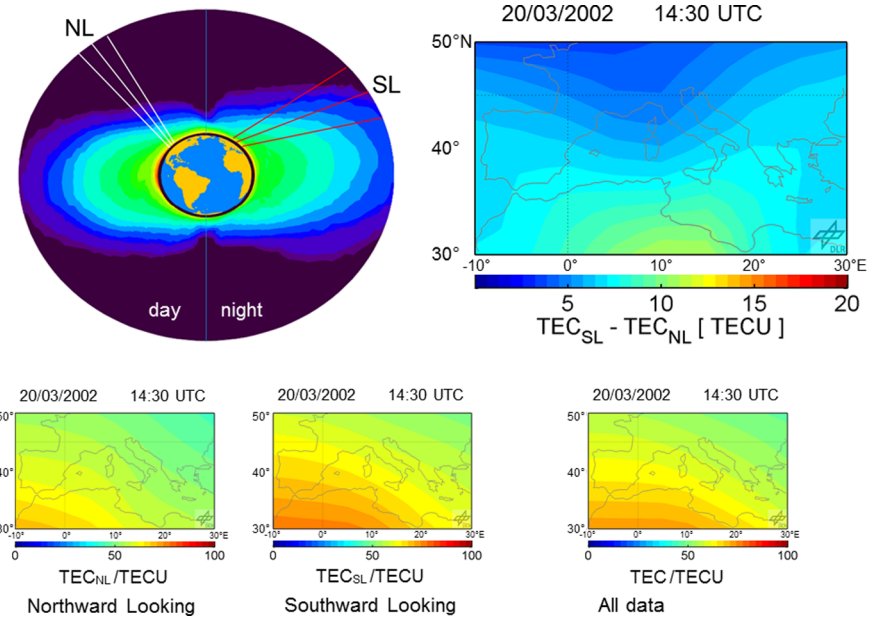

Fig. 1. Illustration of different contributions of the plasmasphere in TEC estimates. Geo-plasma reconstruction sample from CHAMP data (upper panel, left side). TEC estimates from ground based GPS data on March 20, 2002 at 14:30 UT from Northward looking (NL) and Southward looking (SL) satellite links over South-Europe. Corresponding TEC maps (bottom panel left side) in comparison with the differential TEC map (upper panel right side) and the regular TEC map based on a full data set (lower panel right side).

Klobuchar, 1978, 1980), systematic studies including experimental observations and theoretical analysis are needed. Coupling processes between ionosphere and plasmasphere e.g. concerning the thermal structure of the plasmasphere or upward and downward plasma transport are essential to understand ionospheric phenomena. Focusing on Beacon and GNSS measurements, ionospheric phenomena such as nighttime enhancements (e.g. Jakowski et al., 1991), the Weddell Sea anomaly (WSA) as described in several papers (e. g. Horvath & Essex, 2003; He et al., 2009) and the Nighttime Winter Anomaly (NWA) first described by Jakowski et al. (1981, 1986, 2015) are mentioned here.

Besides whistler and in situ measurements on board satellites, radio sounding of the plasmasphere by using coherent dual frequency measurements has been carried out since many years. Thus, the plasmaspheric content could be estimated by comparing differential Doppler and Faraday rotation beacon measurements at signals from geostationary satellites already in the 70s and 80s (e.g. Davies et al., 1976, 1977; Kersley & Klobuchar, 1978, 1980; Jakowski & Kugland, 1982). Nowadays, measurements of the TEC either on ground or on board Low Earth Orbit (LEO) satellites by utilizing dual frequency signals from GPS satellites at about 20200 km orbit height provide essential information on the ionosphere/plasmasphere systems (e.g. Lunt et al., 1999a; Heise et al., 2002; Mazella et al., 2002; Belehaki et al., 2004; Jakowski, 2005; Yizengaw et al., 2008; Mazella, 2009; Lee et al., 2013; Klimenko et al., 2015; Chen & Yao, 2015). Although an increasing number of LEO satellites will be available in the near future being able to receive also signals from other Global Navigation Satellite Systems (GNSS) like GLONASS, Galileo or Beidou, data gaps will occur because operational services rely only on fresh data with low latency. To get a full picture despite challenging operational requirements, data gaps may be filled by model data or by assimilating all available data into a background model. Thus, dual frequency GPS data received on board the LEO satellite CHAMP for navigation has been assimilated into an ionosphere-plasmasphere background model (Heise et al., 2002). The inversion of the TEC data provides a 3D electron density distribution in the vicinity of the CHAMP satellite in a volume that is spanned by all radio links from the LEO satellite to all receivable GPS satellites. After collecting data from a full satellite revolution within about 90 min and assimilation into the background model (Daniell et al., 1995) a complete image of the geo-plasma in the orbit plane from LEO satellite height up to GPS orbit height can be reconstructed as can be seen as a typical sample in Figure 1 (upper left panel). The obtained results indicate several processes such as compression and depletion of the plasmasphere during storms and plasma outflow at high latitudes (Jakowski et al., 2007). The results are consistent with associated radio occultation and ground based measurements. Ground based TEC data may be impacted by the plasmasphere from about 10% up to more than 50% at night (e.g. Lunt et al., 1999b; Chen & Yao, 2015; Klimenko et al., 2015). Thus, in particular at night the often used thin layer approach for mapping measured slant to vertical TEC may cause considerable mapping errors (Jakowski et al., 1996) which are related to an erroneous bias estimation for TEC measurements (Mazella et al., 2002, Mazella, 2009) or to inaccurate range error estimates in positioning. Thus, special care was taken to address the plasmasphere contribution in the Galileo ionospheric correction model NeQuick (e.g. Cueto et al., 2007).

Another mapping error may occur when considering the direction of measured radio links between receiver and GNSS transmitters. This effect is illustrated in Figure 1 where two different data sets have been used to create TEC maps over the

Southern part of Europe. One data set considers only measurements looking northward in the azimuth range ±60° (NL), the other looking southward in the azimuth range 120–240° as illustrated in the upper left panel. As the geometry of the radio links clearly shows, the SL links penetrate the plasmasphere much deeper than the NL measurements do. The underlying geo plasma distribution is a typical sample derived from CHAMP reconstructions (Heise et al., 2002). As a consequence, the associated TEC maps look quite different as seen in the lower panel. The difference of the created maps is shown on the right side in the upper panel. Since the plasmaspheric contribution of up to more than 10 TEC units (1 TECU = 10^{16} m^{-2}) cannot be ignored, the knowledge of the plasmaspheric electron content effect on GNSS signal needs to be considered, especially around solar cycle minimum and at night.

At present days numerous satellites carrying a GNSS receiver on board for navigation purposes can be used for retrieving vertical electron density profiles by means of radio occultation measurements and for imaging the 3D electron density distribution of the topside ionosphere/plasmasphere (TIP) (e.g. Heise et al., 2002; Jakowski et al., 2002a; Chen & Yao, 2015; Klimenko et al., 2015). In case of orbit heights of less than 500 km the plasmasphere content should be included in an appropriate way. Thus, Jakowski et al. (2002a, b) have used a simple TIP model assuming exponential decay with height.

Nowadays the 3 satellites of the ESA satellite mission SWARM can effectively be used to monitor space weather and associated TIP electron density variations (e.g. Stolle et al., 2013). Assimilation of thousands of link related TEC data require a fast and robust background model to respond properly to dynamic processes in the plasmasphere. Based on the experience of fast and robust models developed in recent years for the ionospheric key parameters TEC, NmF2 and hmF2 (Jakowski et al., 2011a; Hoque & Jakowski, 2011, 2012) and their effective use (e.g. Jakowski et al., 2011b) we have started developing a fast and robust plasmasphere model suitable in operational services. After describing the data base in Section 2 in more detail we will present the model algorithm in Section 3 and subsequently discuss modelling results in relation to some ionospheric /plasmaspheric phenomena.

2 Data base

The data base consists of topside reconstructions of the electron density using data from the CHAMP satellite mission in the years 2000–2005. The German CHAMP (CHAllenging Minisatellite Payload) satellite has been launched on 15 July 2000 into a near-Earth polar orbit (inclination 87°) with an initial altitude of 450 km (e.g. Reigber et al., 1996). CHAMP was equipped with dual-frequency GPS receivers for radio occultation measurements and for navigation purposes, in particular for precise orbit determination enabling the computation of the integrated electron density (TEC) along the ray paths between GPS satellites in view and CHAMP (Heise et al., 2002). The number of ray paths between GPS satellites and CHAMP during one orbital revolution was up to 4000 which were non-uniformly distributed according to the visibility of GPS satellites. Therefore, to obtain a complete electron density distribution in the CHAMP satellite orbit plane, TEC data obtained along the different radio links were assimilated into a background model (Parameterized Ionospheric Model; Daniell et al., 1995). The assimilation resulted in a 3D reconstruction of the electron density for each CHAMP revolution close to the CHAMP orbit plane. Considering the revolution time of about 93 min, 15–16 reconstructions have been obtained per day. Starting from 2000, DLR Neustrelitz has collected more than 30 000 electron density reconstructions of the TIP. A typical TIP reconstruction can be seen in Figure 1 (top left) to illustrate the contribution of the plasmasphere in ground based GNSS measurements. The global view on the Earth's plasma environment up to GPS orbit heights illustrates the high potential for studying magnetospheric-ionospheric coupling processes (e.g. Jakowski et al., 2007).

Validation of the electron density reconstructions was made using in-situ plasma density measurements of the Planar Langmuir Probe installed on board CHAMP and incoherent scatter measurements at different sites. Compared with the Langmuir Probe data, the assimilation results have practically no bias and agree quite well within a standard deviation of 2×10^{11}m^{-3} (Heise et al., 2002). These data sets form the basis for comparative and validation studies e.g. with topside data from IRI-2007 and other models (Mayer & Jakowski, 2007). A previous validation of these GNSS derived plasmasphere data from CHAMP with plasmasphere density profile data from the IMAGE/RPI measurements have shown a good agreement up to about $L = 3$ (Gerzen et al., 2015).

The solar activity level is approximated by the solar radio flux index F10.7 measured in solar flux units (1sfu = 10^{-22} Wm^{-2} Hz^{-1}).

3 Modelling approach

Our plasmasphere model approach consists of two parts, a high altitude part where plasmaspheric processes related to plasmapause and magnetosphere dominate and a lower part where ionospheric coupling is taken into account. The electron density distribution in the high altitude plasmasphere is closely related to geomagnetic field lines which can be considered in a first order approach as isolines of the electron density. Therefore, the high altitude modelling approach refers to the McIllwain parameter L. The basic assumption follows a simplifying exponential decay of the electron density in the geomagnetic equatorial plane as a function of L (e.g. Carpenter & Anderson, 1992; Lemaire & Gringauz, 1998) as represented by:

$$N_{ePL} = N_{ePL1} \cdot \exp\left(\frac{R_E(1-L)}{H_{PL}}\right) \quad (1)$$

N_{ePL1} means here formally the electron density at the Earth surface at $L = 1$, H_{PL} is the corresponding plasma scale height. To keep the plasmasphere model as simple as possible, we define (1) as the basic approach for the upper part of the model.

For the lower part the electron density is also described by an exponential decay but as a function of height h as already utilized in former approaches (Jakowski et al., 2002a,b):

$$N_{ePh} = N_{ePh0} \cdot \exp\left(-\frac{h}{H_{Ph}}\right) \quad (2)$$

N_{ePh0} means here formally the electron density at the Earth surface at $h=0$, H_{Ph} is the corresponding plasma scale height. Principally, the lower boundary of the plasmasphere is fixed at 1000 km height that corresponds approximately to the transition height h_T where $[O^+]=[H^+]$. This is a pragmatic approach, allowing an easy use of the model in operational applications. Finally the electron density N_{eP} of the plasmasphere is given by the sum of the electron densities of both parts.

$$N_{eP} = N_{ePh} + N_{ePL} \tag{3}$$

3.1 High altitude part of the plasmasphere model as a function of *L*

The relationship between L, the height h above the Earth surface and the geomagnetic latitude ϕ_m is given by:

$$L = \frac{R_E + h}{R_E \cos^2(\phi_m)} \tag{4}$$

To extract plasmasphere information from TIP reconstructions based on CHAMP data we assume a lower limit of altitude $L_{\min}=1.5$ to avoid overlapping in the lower plasmasphere with ionosphere controlled densities. The upper limit is formally given by $L \approx 3$ according to the results of a comparative study of CHAMP topside reconstructions with IMAGE data (Gerzen et al., 2015). Thus, for the high altitude part model coefficients are derived from CHAMP data obtained in the range $1.5 \le L \le 3$. Plasmaspheric densities at higher L shells than $L=3$ are extrapolated based on formula approaches derived for L in the range $1.5 \le L \le 3$. Principally, the upper boundary is defined by the height of the plasmapause that may vary as a function of space weather conditions (Menk et al., 2014). In this preliminary model the plasmapause position L_{pp} is fixed at $L_{pp}=5$ assuming geomagnetically quiet conditions. Following equation (4) we get for the radial distance of the plasmapause R_{PP} in the equatorial plane:

$$R_{PP} = L_{PP} \cdot R_E \cdot \cos^2(\phi_m) \tag{5}$$

Assuming that the plasmapause maps down to the ionosphere along the field line and the plasmapause may reduce to $L_{pp}=3$ or even less, we model the high altitude plasmasphere part between geomagnetic latitudes ±20° at the Northern and Southern hemispheres.

Taking into account these input data restrictions we have derived the key parameters N_{ePL1} and H_{PL} in equation (1) from CHAMP reconstruction data. As Figure 2 shows, scale height H_{PL} and base density N_{ePL1} can be derived from the slope and crossing values at $L=1$, respectively of the fitted curve.

The modelling approach for N_{ePL1} follows successful approaches used in TEC, NmF2 and hmF2 modelling (Jakowski et al., 2011a; Hoque & Jakowski, 2011, 2012). So the base density N_{ePL1} is defined by the product of F_i terms:

$$N_{ePL1} = F_1^{NL} \cdot F_2^{NL} \cdot F_3^{NL} \quad [\text{in units of } 10^{12}\,\text{electrons/m}^3] \tag{6}$$

Here the local time (LT) dependency of F_1^{NL} is modeled by:

$$F_1^{NL} = \cos\chi^{***} + (c_1\cos(DV) + c_2\sin(DV) + c_3\cos(SDV) + c_4\sin(SDV)) \cdot \cos\chi^{**} \tag{7}$$

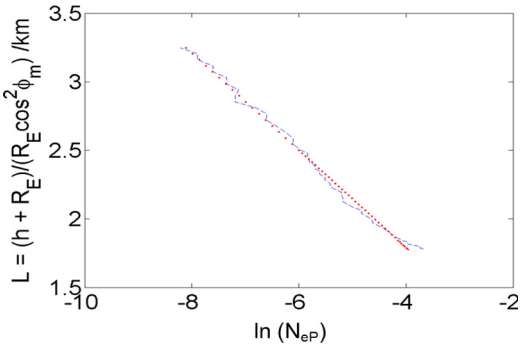

Fig. 2. Semi-logarithmic sample plot of the electron density N_{eP} from CHAMP (dashed blue) as a function of L approximated by a straight line (dotted red) whose constant slope is directly related to the scale height H_{PL}.

Where the diurnal variation (DV), the semi-diurnal variation (SDV) and the ter-diurnal variation (TDV) which is used later are defined by:

$$DV = \frac{\pi}{12} \cdot LT \quad SDV = \frac{\pi}{6} \cdot LT \quad TDV = \frac{\pi}{4} \cdot LT \tag{8}$$

The solar zenith angle (χ) dependency from the declination of the sun (δ) and the geographic latitude (ϕ) is considered by the following expressions following Jakowski et al. (2011a).

$$\cos\chi^{*} = \cos(\phi - \delta) \tag{9}$$

$$\cos\chi^{**} = \cos\chi^{*} - \frac{2\phi}{\pi}\sin\delta \tag{10}$$

$$\cos\chi^{***} = \cos\chi^{*} + P_{F1} \tag{11}$$

P_{F1} is a fixed parameter.

The annual/semiannual variation (AV/SAV) F_2^{NL} is defined by:

$$F_2^{NL} = 1 + c_5\cos(AV) + c_6\sin(AV) + c_7\cos(SAV) + c_8\sin(SAV) \tag{12}$$

$$\text{with} \quad AV = \frac{doy}{365.25} \cdot 2\pi \quad \text{and} \quad SAV = \frac{doy}{365.25} \cdot 4\pi \tag{13}$$

Finally, the dependence from solar activity approximated by F10.7 is considered by F_3^{NL} according to:

$$F_3^{NL} = c_9 + c_{10}F10.7 \tag{14}$$

Using this approach the fitting is quite successful as the upper panel in Figure 3 shows.

For the plasmaspheric scale height H_{PL} we apply a similar approach for the diurnal and seasonal variation and dependence from solar activity ignoring the dependence from geomagnetic latitude via

$$H_{PL} = F_1^{HL} \cdot F_2^{HL} \cdot F_3^{HL} \tag{15}$$

The local time variation term F_1^{HL} is defined by:

$$F_1^{HL} = 1 + (c_{11}\cos(DV) + c_{12}\sin(DV) + c_{13}\cos(SDV) + c_{14}\sin(SDV)) \cdot \cos\chi^{**} \tag{16}$$

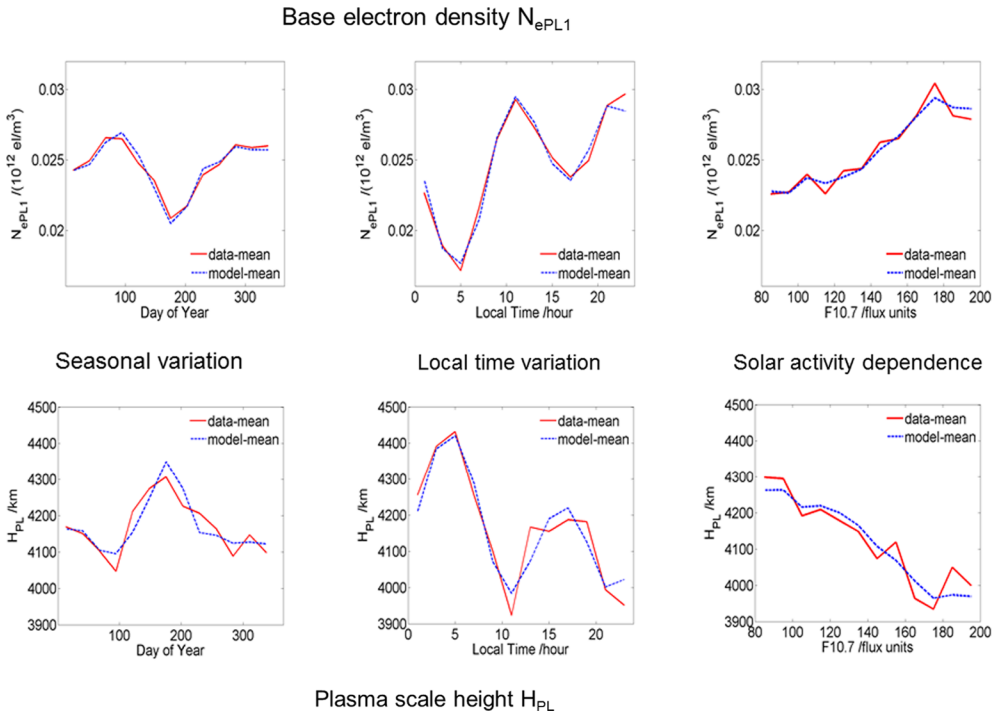

Fig. 3. Fitting results for base electron density N_{ePL1} and H_{PL} considering the seasonal and local time dependence and dependence from solar activity provided by the F10.7 index. Arithmetic means are computed for time intervals of 27 days data and model covering all years.

The annual/semiannual variation term F_2^{HL}:

$$F_2^{HL} = 1 + c_{15}\cos(AV) + c_{16}\sin(AV) + c_{17}\cos(SAV) + c_{18}\sin(SAV) \quad (17)$$

Finally, the dependence from solar activity is again approximated by F10.7:

$$F_3^{HL} = c_{19} + c_{20}F10.7 \quad (18)$$

After fitting these approaches to the CHAMP based TIP reconstructions we obtain the coefficients $c_1 \ldots c_{20}$ for modeling the L shell depending base density N_{ePL1} and plasma scale height H_{PL}. A few results are shown in Figure 3, lower panel.

It is interesting to note that the seasonal, diurnal and solar activity dependencies of N_{ePL1} and H_{PL} are practically in antiphase. This behavior reduces the related variability of the electron density but indicates a change of the vertical plasma distribution as will be discussed in the subsequent section in more detail.

As mentioned before, the derived plasma scale height parameter H_{PL} is assumed to be constant up to the plasmapause height at L_{PP}. To describe the drop of electron density at the plasmapause up to about two orders of magnitude in the equatorial plane we use a dimensionless factor F_{PP} that depends only on height h and the selected plasmapause height L_{PP} or R_{PP} defined by equation (5).

For this study L_{PP} is fixed at $L_{PP} = 5$ and $R_E = 6371$ km. The L_{PP} value is planned to be determined later by a plasmapause model that is currently under development. Since this simplification has no big effect on the electron content (<1 TECU) the presented model can already be used in GNSS applications where the bias estimates might have bigger errors.

Defining F_{PP} by:

$$F_{PP} = arctan\left(\frac{\left(\frac{(R_{PP}-R_E-h)}{500}\right)}{\pi}\right) + 0.5 \quad (19)$$

we get for the L shell dependence of the electron density from (1):

$$N_{ePL} = N_{ePL1} \cdot F_{PP} \cdot \exp\left(\frac{R_E(1-L)}{H_{PL}}\right) + N_{eMS} \quad (20)$$

where N_{eMS} is the electron density outside the plasmapause in the magnetosphere assumed to be fixed at $1 \times 10^7\,\mathrm{m}^{-3}$. As in case of fixed L_{pp} definition this value has no practical consequences in GNSS applications.

3.2 Modelling the plasmasphere below about 2000 km as a function of height *h*

Now we describe the lower part of the plasmasphere model at altitudes ≤2000 km in the equatorial plane. Because this altitude range is expected to be impacted by ionospheric coupling the modelling approach is now based on height dependence.

$$N_{ePh0} = F_1^{Nh} \cdot F_2^{Nh} \cdot F_3^{Nh} \cdot F_4^{Nh} \cdot F_5^{Nh} \quad (21)$$

Concerning the local time variation of the ionosphere we include here also the ter-diurnal variation in (8). To keep the number of coefficients small we have fixed the phases based on given optimization. So we get for the local time variation

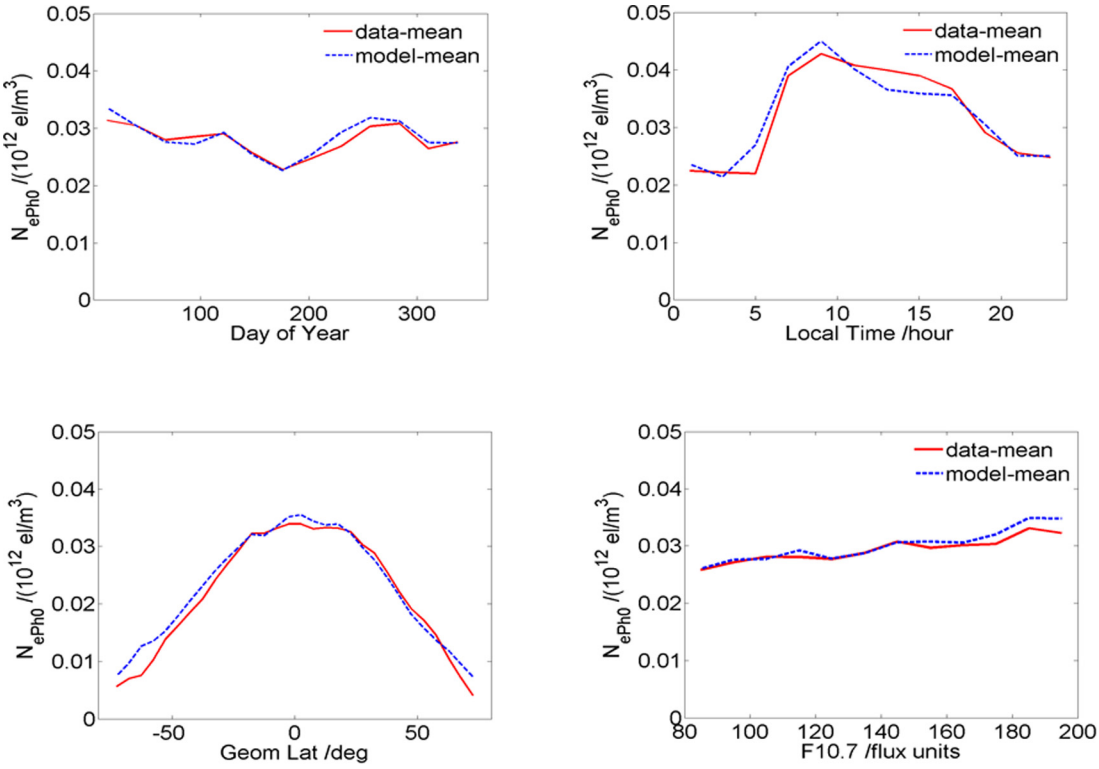

Fig. 4. Fitting results for N_{ePh0} considering the seasonal, local time dependence, geomagnetic latitude dependence and dependence on solar activity index F10.7. Arithmetic means are computed for time intervals of 27 days data and model covering all years.

F_1^{Nh} the expression:

$$F_1^{Nh} = \cos\chi^{***} + (c_{21}\cos(DVm) + c_{22}\cos(SDVm) + c_{23}\cos(TDVm))\cdot\cos\chi^{**} \quad (22)$$

where the modified diurnal, semi-diurnal and ter-diurnal variations *DVm*, *SDVm* and *TDVm* are defined in analogue form as in (8) but include fixed phases not specified here.

The annual and semiannual variation in (12) and (13) are also modified by fixed phases leading to the expression for F_2^{Nh}:

$$F_2^{Nh} = 1 + c_{24}\cos(AVm) + c_{25}\cos(SAVm) \quad (23)$$

Else as in case of the upper part model, here we model the geomagnetic dependency of N_{ePh0} by the expression:

$$F_3^{Nh} = 1 + c_{26}\cos(\phi_m) + c_{27}(\cos(4\phi_m))^2 \quad (24)$$

Since the north- and southward crests are explicitly visible due to ionosphere coupling they are considered by Jakowski et al. (2011a) via the approach:

$$F_4^{Nh} = c_{28}\exp\left(-\frac{(\phi_m - \phi_{c1})^2}{2(\sigma_{c1})^2}\right) + c_{29}\exp\left(-\frac{(\phi_m - \phi_{c2})^2}{2(\sigma_{c2})^2}\right) \quad (25)$$

The coefficients c_{28} and c_{29} take into account the hemispherical asymmetry that has been shown in many observations (e.g. Denton et al., 1999). A comparison of c_{28} and c_{29} can provide such information. The locations ϕ_{c1} and ϕ_{c2} of the crests as well as the half widths σ_{c1} and σ_{c2} have been iteratively optimized.

As before, the solar activity dependence follows a linear approach with F10.7.

$$F_5^{Nh} = c_{30} + c_{31}\cdot F10.7 \quad (26)$$

Selected results of fitting this approach to CHAMP based reconstructions at altitudes between 600 and 2000 km height depending on the latitude are shown in Figure 4.

Because the data stem from the Northern and Southern hemispheres, the averaged N_{ePh0} is practically constant over the year, indicating a small minimum in Northern summer and a maximum in Northern winter. Diurnal, latitudinal and solar activity dependencies behave as expected, closely related to the solar illumination and activity. It is interesting to note that the diurnal maximum appears already in the early morning hours just after sunrise and before 10 *LT*. This is probably a result of an enhanced uplifting of atomic oxygen ions in the early morning hours between 4 and 8 *LT*.

The latitudinal variation slightly indicates the crest regions at both sides of the geomagnetic equator at around 20°. The model approach follows all these variations.

To complete the model we have still to consider the plasma scale height H_{Ph} whose modeling approach follows the same guidelines as considered before according to:

$$H_{Ph} = F_1^{Hh}\cdot F_2^{Hh}\cdot F_3^{Hh}\cdot F_4^{Hh} \quad (27)$$

So the local time dependency F_1^{Hh} is expressed in a similar way as in (22) as follows:

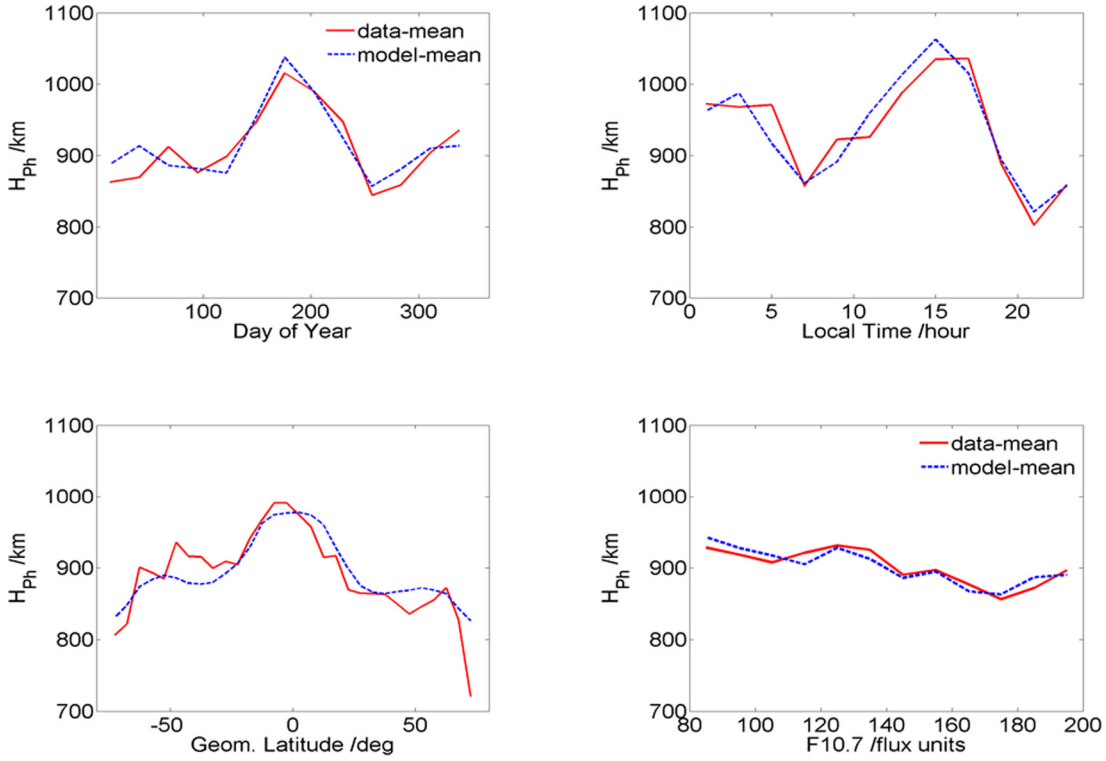

Fig. 5. Fitting results for the scale height H_{Ph} considering the seasonal, local time, geomagnetic latitude dependence and dependence on solar activity index F10.7. Arithmetic means are computed for time intervals of 27 days data and model covering all years.

$$F_1^{Hh} = 1 + (c_{32}\cos(DVm) + c_{33}\cos(SDVm) + c_{34}\cos(TDVm))\cdot\cos\chi^{**} \quad (28)$$

with modified values for the diurnal, semi-diurnal and ter-diurnal variations by including fixed phases that have been iteratively optimized.

The annual/semiannual variation is defined in the same way as in (23) by:

$$F_2^{Hh} = 1 + c_{35}\cos(AVm) + c_{36}\cos(SAVm) \quad (29)$$

The dependency on the geomagnetic latitude is defined by:

$$F_3^{Hh} = 1 + c_{37}\cos(0.7\phi_m) + c_{38}(\cos(2.8\phi_m))^2 \quad (30)$$

Again, the dependence form the solar activity follows the same linear approach as used in previous cases:

$$F_4^{Hh} = c_{39} + c_{40}\cdot F10.7 \quad (31)$$

Selected results of the data fitting to this modeling approach are shown in Figure 5.

It is interesting to note that the scale height has a clear maximum in Northern summer indicating a certain asymmetry of the plasmasphere when comparing the Northern and Southern hemispheres. The plasmaspheric scale height shows a minimum in the early morning hours just after sunrise and before 10 *LT* exactly in antiphase with N_{eP0} followed by a maximum in the afternoon at about 15–16 *LT*. This behavior nicely demonstrates the filling process of the plasmasphere from below starting with high N_{ePh0} and low scale heights. In the course of the day the filling process leads to growing scale heights and the maintenance of a high N_{ePh0} level as seen in Figure 4. The scale height dependence from the geomagnetic latitude has a clear maximum at the geomagnetic equator that can easily be explained by the equatorial anomaly mechanism that describes a strong uplifting at the geomagnetic equator to form the Northern and Southern crests. The two secondary maxima at around ±60° N geomagnetic latitude indicate another plasma filling mechanism that will be discussed in Section 4 in more detail. The anticorrelation of the scale height with solar activity is unexpected because the plasma temperature increases with growing solar activity. To explain the anticorrelation it is assumed that dynamic plasma filling processes from below dominate over equilibrium conditions that would result in a positive correlation of H_{Ph} and F10.7. The model approach follows all observed variations.

4 Results and discussion

According to (3) the total electron density N_{eP} is defined by the sum of the high altitude L shell depending part and the lower height depending part of the plasmaspheric model from 1000 km upward according to $N_{eP} = N_{ePh} + N_{ePL}$.

Some results concerning the diurnal variation of the plasmaspheric electron content derived from the full model at low and high solar activity conditions are shown for the starting heights 1000 and 2000 km in Figures 6–8. As mentioned before, we consider the 1000 km height as the fixed plasmasphere base level. The vertical integration of the

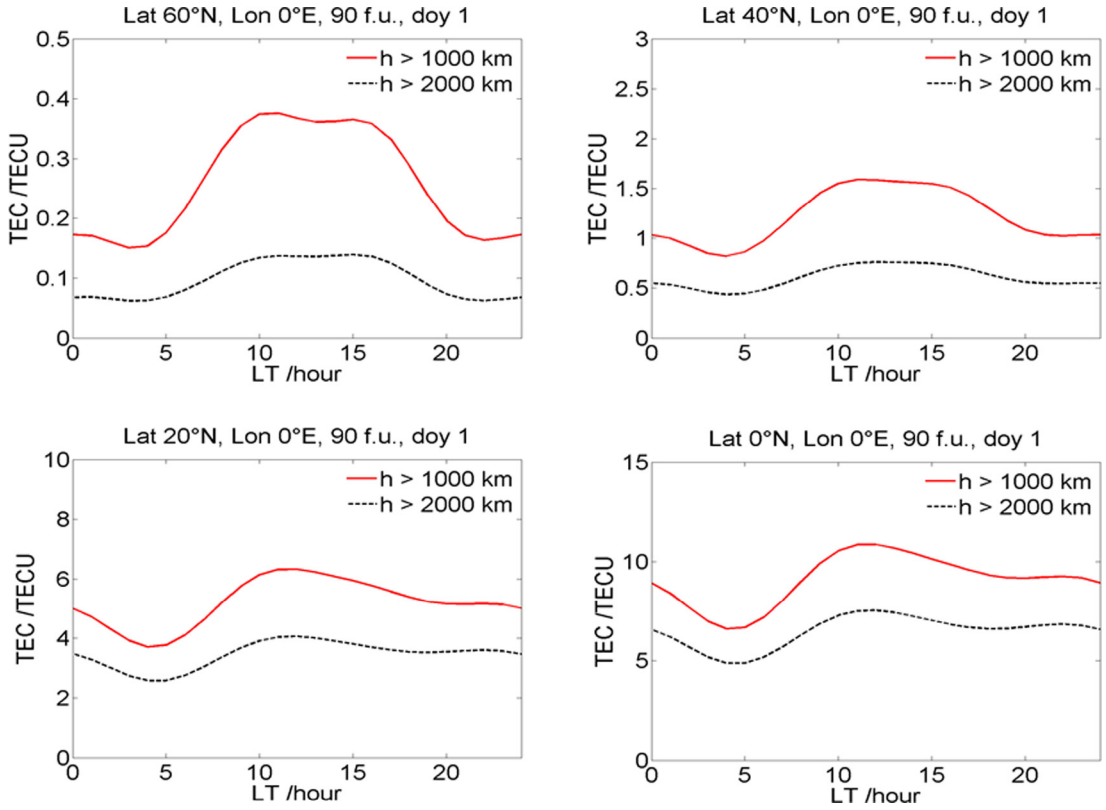

Fig. 6. Vertical TEC of the plasmasphere from 1000 km (red line) and 2000 km (black dotted line) upward at geographic latitudes $\phi = 60, 40, 20$ and 0° N along the geographic longitude $\lambda = 0°$ E for low solar activity conditions (F10.7 = 90).

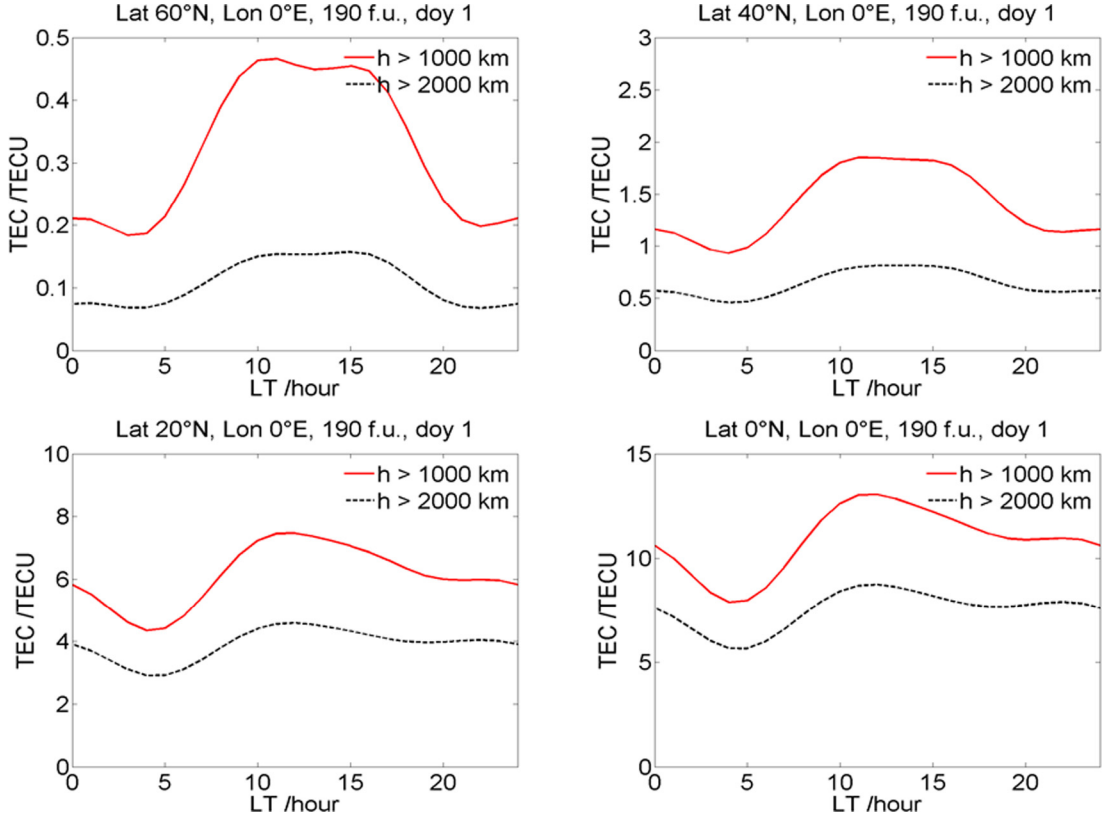

Fig. 7. Vertical TEC of the plasmasphere from 1000 km (red line) and 2000 km (black dotted line) upward at geographic latitudes $\phi = 60, 40, 20$ and 0° N along the geographic longitude $\lambda = 0°$ E for high solar activity conditions (F10.7 = 190).

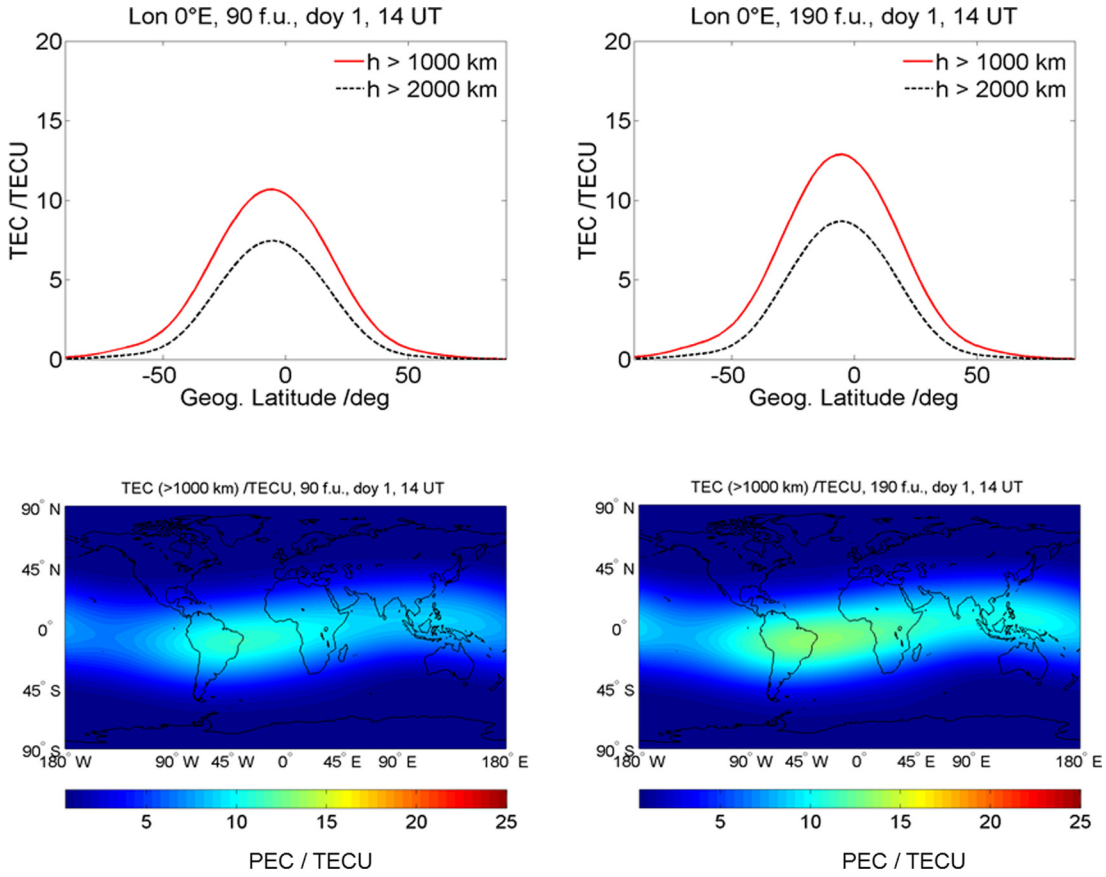

Fig. 8. Upper panel: Vertical TEC of the plasmasphere from 1000 km (red line) and 2000 km (black dotted line) upward as a function of geographic latitudes along the geographic longitude $\lambda = 0°$ E for low and high solar activity conditions. Lower panel: Global maps of PEC at 14:00 UT under low (F10.7 = 90) and high solar activity conditions (F10.7 = 190).

electron density from 1000 km upward provides an electron content that we specify here as plasmasphere electron content (PEC). In addition we have selected the 2000 km height level because former Faraday rotation measurements at linearly polarized VHF signals transmitted from geostationary satellites can be considered to measure TEC up to about 2000 km height. Due to this fact a comparison with simultaneous modulation phase delay measurements enabled the estimate of the plasmaspheric content above 2000 km height already in the 70s and 80s (e.g. Davies et al., 1977; Kersley & Klobuchar, 1978, 1980; Jakowski & Kugland, 1982). Considering the permanent slant ray path geometry to geostationary satellites from mid-latitude stations, the estimate of a few TECU is in general agreement with averaged results presented in Figures 6–8. When using early beacon measurements of Navy Navigation Satellite System (NNSS) satellites at orbit heights of about 1000 km for a comparison with modulation phase delay measurements at geostationary satellites and later with GPS measurements, a direct estimate of PEC has been made in several beacon studies (e.g. Davies et al., 1977; Ciraolo & Spalla, 1997; Lunt et al., 1999a). The PEC values shown in Figure 8 agree quite well with former estimations of plasmaspheric TEC reported in the beacon literature and also with more recent estimates (e.g. Mazella et al., 2002; Huang et al., 2004; Chen & Yao, 2015; Klimenko et al., 2015).

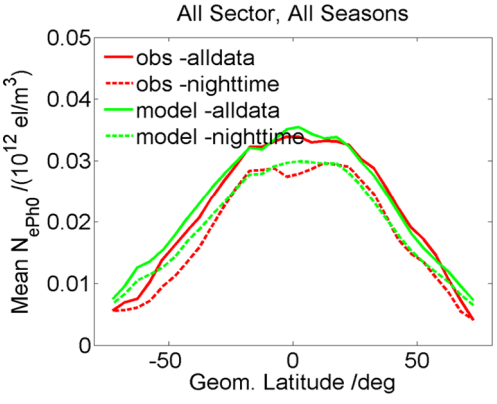

Fig. 9. Fitting results for the geomagnetic latitude dependence of N_{ePh0} including all data (full line) and for nighttime conditions (dotted) in comparison with related model results (green).

Compared with the ionosphere the diurnal variation of TEC in the plasmasphere is rather low. Nevertheless, there is a rapid increase in the morning hours just after sunrise up to about 10 *LT*. Subsequently, the reached TEC level decreases slowly at lower latitudes whereas with increasing latitude the diurnal variation follows more and more the ionospheric *LT* dependence. It should be mentioned that the daily minimum of

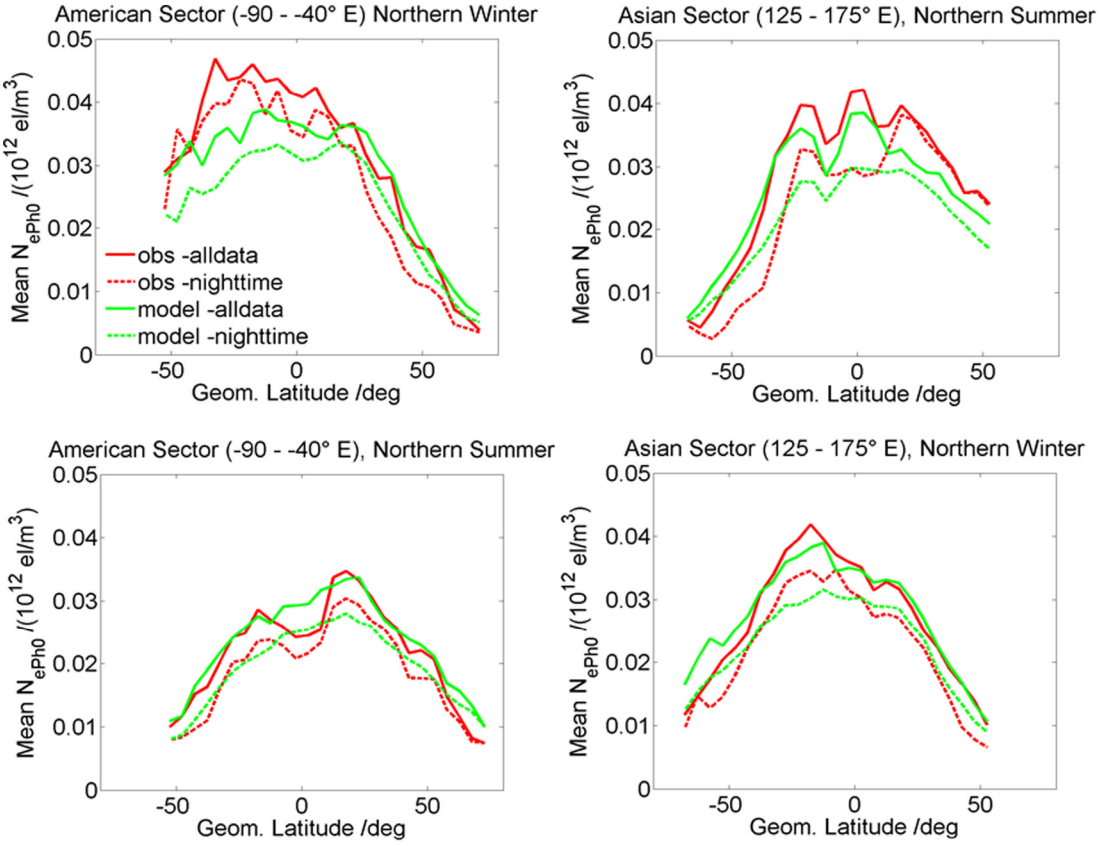

Fig. 10. Fitting results for the geomagnetic latitude dependence of N_{ePh0} including all data (full line) and for nighttime conditions (dotted) in comparison with related model results (green).

TEC just before sunrise is rather stable at the same geomagnetic latitude and independent from solar activity whereas the diurnal maximum increases slightly with solar activity in particular when we consider the 1000 km base level. Due to the low sensitivity to solar activity changes and delayed response via coupling processes it is recommended to run the model with an average value of F10.7 (e.g. monthly average) instead of the actual F10.7 index. Summarizing, it can be concluded that the model provides TEC estimates which are in principal agreement with the current knowledge of the plasmaspheric electron content behavior.

Since the lower part of the plasmasphere below about 2000 km height contributes significantly more to the PEC than the upper part, we will discuss these input data for the model in more detail. The overall fitting of the model coefficients for N_{ePh0} is shown in Figure 9 including a separate data set for nighttime conditions. It can be seen that for the entire data set the geomagnetic dependence of N_{ePh0} is practically symmetric at both sides of the geomagnetic equator as it has been shown already in Figure 4. Here we see that this conclusion is also valid for nighttime conditions at a lower level of N_{ePh0}. The crests are somewhat pronounced at around ±20° geomagnetic latitude, i.e. slightly poleward shifted when referring to their location at about ±15° in the ionosphere. A light shoulder is indicated at around ±60°. More pronounced maxima have been discussed for H_{Ph} in the previous section when describing Figure 5. Although this dependency is rather small, the model approach follows these variations with geomagnetic latitude.

To explain this shoulder in N_{ePh0} in Figure 9 and the appearance of secondary maxima of H_{Ph} in Figure 5 at about 60° we assume an enhanced filling of the plasmasphere from ionospheric heights. Such a mechanism has been recently described by Jakowski et al. (2015) to explain some ionospheric anomalies such as the NWA discovered by Jakowski et al. (1981) and the midsummer nighttime anomaly (MSNA) as described by Lin et al. (2010). Specific forms of the MSNA are the WSA and the Ochotsk Sea Anomaly (OSA) (e.g. Horvath & Essex, 2003; Natali & Meza, 2013; Meza et al., 2015). Following this argumentation it is supposed that in particular equatorward blowing meridional winds in the summer hemisphere lift up ionospheric plasma very effectively at such longitude sectors where geographic latitudes significantly exceed geomagnetic latitudes. Due to the tilted geomagnetic dipole this appears in particular at the American sector in the southern hemisphere and at the Asian sector in the Northern hemisphere. Whereas at daytime the plasma escapes towards plasmaspheric heights it returns in the evening hours and creates a diurnal ionization maximum observable in the WSA and OSA at the local ionosphere. Due to the enhanced plasma pressure in the field tubes a part of the uplifted plasma is able to cross the equator along the field lines and feed the nighttime winter ionosphere, thus creating the NWA effect that is clearly visible at low solar activity (LSA) conditions (Jakowski et al., 1981; Jakowski & Förster, 1995; Natali & Meza, 2013; Jakowski et al., 2015) at the American (North-America) and Asian (Australia) sectors. This process is

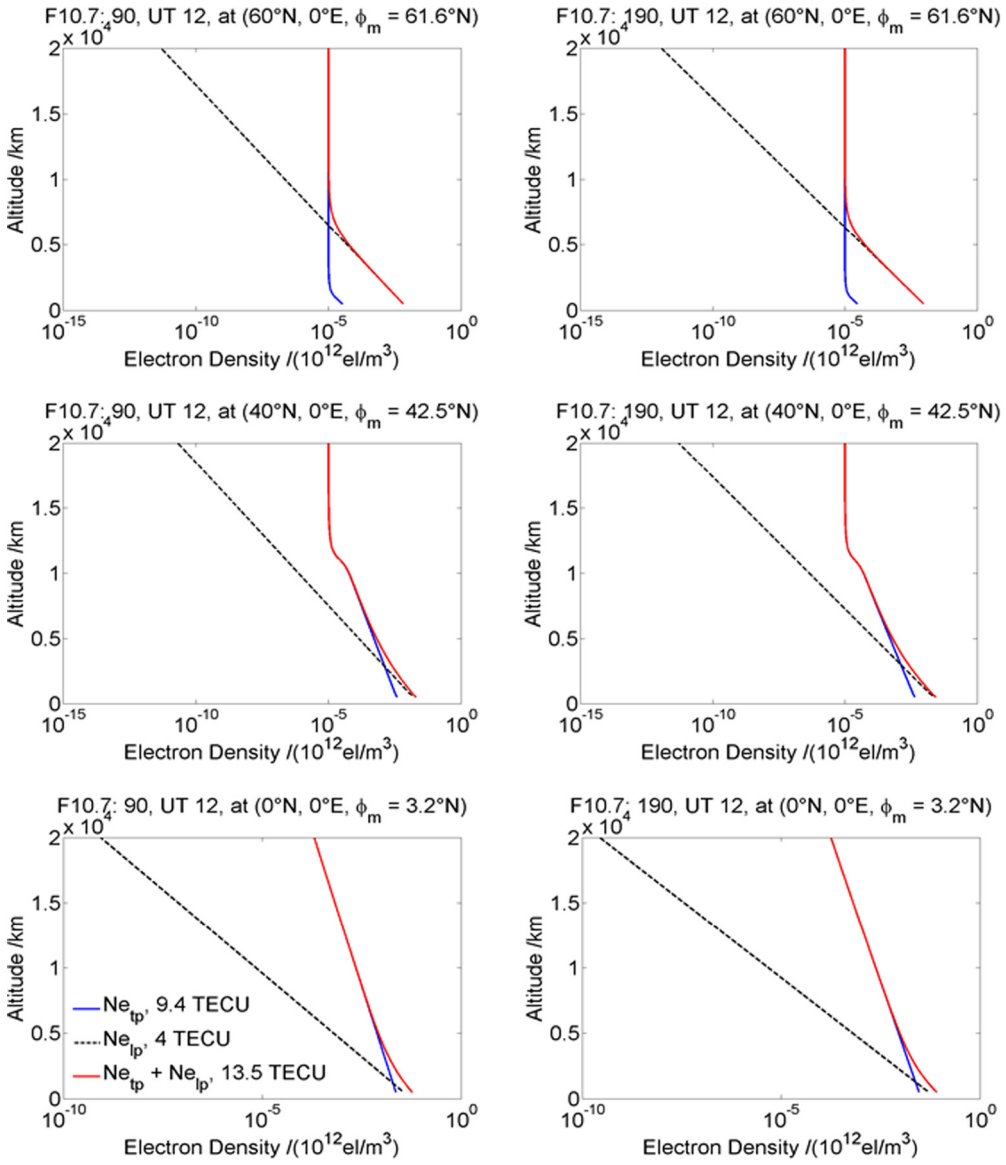

Fig. 11. Semi-logarithmic plots of the height dependence of the electron density at different latitudes under low and high solar activity (LSA and HSA, respectively) conditions. Dotted black line corresponds with the scale height of the lower part H_{Ph}; the blue line corresponds with the scale height of the upper part H_{PL}; the red line is the sum of both contributions.

confirmed by CHAMP measurements used for our model approach as seen in Figure 10. Both upper panels represent conditions as discussed above suited to observe the MSNA in the southern hemisphere at the American sector (WSA) and in the northern hemisphere at the Asian sector (OSA). In the conjugated winter hemispheres one should observe the NWA effect under LSA conditions. The upper plots are characterized by a strong asymmetry of the N_{ePh0} behavior concerning the geomagnetic latitude. The summer hemispheres show much higher N_{ePh0} values than the corresponding winter hemispheres thus supporting strong plasma uplifting. The asymmetry disappears half a year later (cf. both lower panels) indicating that the strong uplifting mechanism in the summer hemispheres at North America and over Australia does not work due to opposite different geomagnetic – geographic relationships (here geomagnetic latitudes exceed corresponding geographic latitudes). Both findings further support the mechanism suggested by Jakowski et al. to explain the NWA (Jakowski et al., 1981; Förster & Jakowski, 1988; Jakowski & Förster, 1995) and associated with this, also the MSNA (Jakowski et al., 2015). Since the modelling approach follows the input data quite well, it can be stated that the Neustrelitz plasmasphere model (NPSM) includes the NWA and MSNA phenomena such as the WSA and OSA to a certain degree.

The model provides a three dimensional distribution of the electron density on global scale. An impression of the height dependence of the electron density distribution provided by the two model parts is shown in Figure 11. The semi-logarithmic plots of the electron density as a function of height at different latitudes along the 0° E meridian indicate both parts by different scale heights expressed by two straight lines with

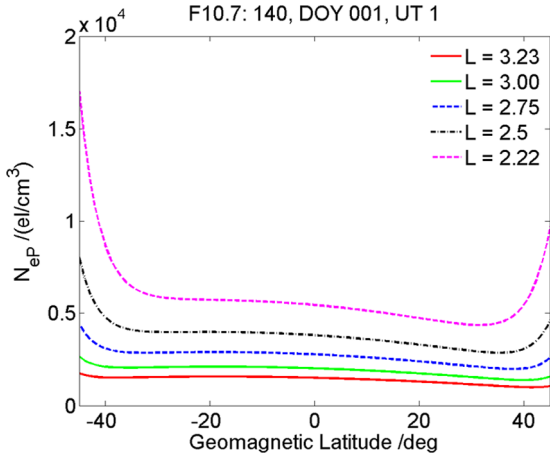

Fig. 12. Plasmaspheric electron density along different L shells as a function of geomagnetic latitude. The sample is computed for doy 001, UT = 01:00 at a solar activity level of F10.7 = 140.

different slopes (the dotted black line for H_{Ph}, the full blue line for H_{PL}). In addition to this also the plasmapause is indicated by a rapid fall of the electron density to the constant outside level of 1×10^7 m^{-3}. At geomagnetic latitudes of about 60° the plasmapause maps down to the ionosphere thus contributing to the establishment of the mid-latitude trough. At low latitudes the plasmapause at $L_{pp} = 5$ is outside the figure. Since the electron density distributions provided by both model parts are simply added to form the total electron density of the entire model, this might lead to problems due to overlapping. As can be seen in the mid and lower panels, the transition region between both model approaches is rather small, i.e. both parts are practically decoupled because of quite different scale heights.

The electron density distribution as a function of height can also be presented as a function of L shells as shown in Figure 12. The plots illustrate the basic idea that the electron density in the upper part is L shell dependent considering the L shells as isolines whereas it is height dependent in the lower part. Coming closer to the Earth, dynamic coupling processes with the ionosphere have to be taken into account as has been discussed already and the radial height dependence becomes more and more important as can be seen at lower L shells with increasing geomagnetic latitudes. It should be mentioned that the electron density distribution shown in Figure 12 is very similar to those derived from IMAGE satellite data published by Huang et al. (2004) thus confirming our results. This finding agrees very well with the results of a comparative study of CHAMP based TIP electron density reconstructions with IMAGE data by Gerzen et al. (2015). It was shown that both data sources are similar at L shells less than 3. Thus, the similarity of modeling results presented in Figure 12 with IMAGE data is consistent with results of the comparative study. The asymmetry of both hemispheres is due to the seasonal variation showing higher electron density values in summer than in winter (e.g. Chen & Yao, 2015) and also can be seen in Figures 8 and 10.

Let's check now whether the solar wind induced plasmaspheric compression at the dayside as it can be seen in Figure 1 (upper panel, left side) is also visible in the model. Since the compression is more pronounced at higher L-shells, we cannot expect too much in this respect because the model coefficients are derived from data at L shells ≤ 3. Nevertheless, as seen in Figure 13, the effect is somewhat visible because the nighttime values at 12 000 km height reach almost the daytime values although the base densities at 1000 km height are lower than at daytime. This behavior indicates a daytime compression of the plasmasphere at higher L-shells. This is in principal agreement with the high N_{ePL1} values before midnight and the scale height maximum after midnight as shown in Figure 3.

To get a better visual impression of the general behavior of the geo-plasma environment from the base level at 1000 km upward, Figure 14 shows the electron density distribution in a meridional plane along 110°/290° E that is in general comparable with the CHAMP data based reconstruction shown at the left side. Although less pronounced we see also a slight day-night asymmetry in the NPSM data at the GPS orbit height. Both plots differ in the base level. Electron density reconstructions from CHAMP data start at the satellite orbit height at around 400 km whereas the NPSM base level is fixed at 1000 km height.

5 Summary and conclusions

For better estimating the plasmasphere electron content in operational space weather monitoring and ionospheric corrections of ground based GNSS measurements we have developed an empirical model of the plasmasphere called NPSM. The empirical model provides electron densities from 1000 km height up to GNSS orbit heights. The developed model algorithm is part of a family of empirical models describing key observables of the ionosphere such as TEC, NmF2 and hmF2 using only the solar radio flux index F10.7 as external input parameter. As required for the other models developed in DLR, NPSM shall provide a robust, fast and sufficiently accurate approach of the plasmaspheric electron density to be used as background model for fast reconstructions of the electron density or TEC in near real time GNSS application and services. Considering the family of these models, NPSM is an important step on the way forward to develop a global 3D model suitable in particular for operational space weather services and GNSS applications. The current model approach utilizes electron density reconstructions of the TIP systems derived from dual frequency GPS navigation measurements on board CHAMP from 2000 to 2005 that includes the maximum of solar cycle 23. These data have been shown to agree quite well with plasmaspheric densities derived from IMAGE/RPI data at L shells ≤ 3. Hence, the fitting of the model algorithm is constrained up to $L = 3$ as an upper boundary. The basic model algorithm consists of two exponential decay functions for the electron density; the upper one depending on L-shell values in the geomagnetic equatorial plane, the lower one, altitude depending due to non-negligible ionosphere coupling. To reach GNSS orbit heights at about 20 200 km height we extrapolate the exponential decay derived for the L-shell dependent upper part of the model in the L shell range $1.5 \leq L \leq 3$ up to a fixed plasmapause at $L_{PP} = 5$. Due to the strong coupling with the ionosphere the lower part of the model starting at 1000 km height follows an altitude

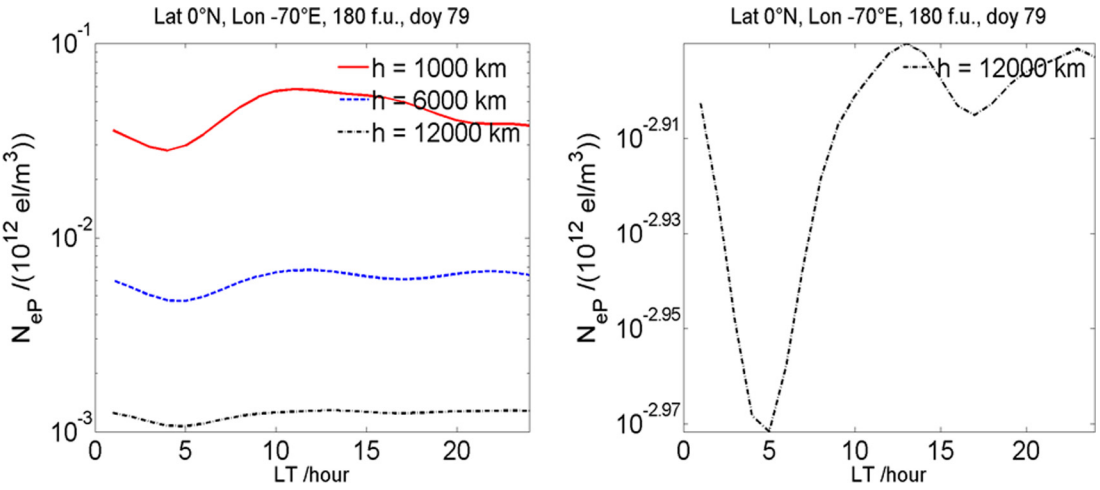

Fig. 13. Diurnal variation of the plasmaspheric electron density for doy 79 at 0° N/70° E at 1000, 6000 and 12 000 km height under HSA conditions (left panel). Zoomed curve for 12 000 km height at the right panel.

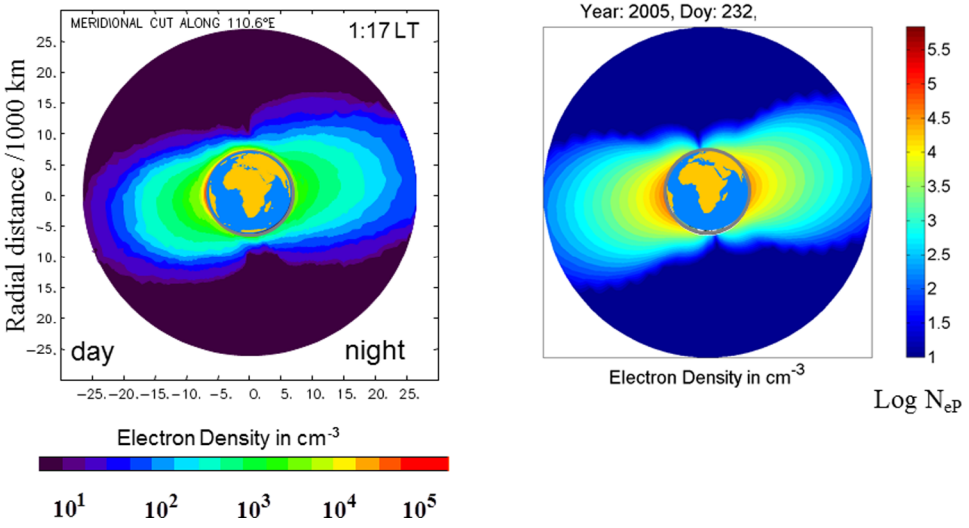

Fig. 14. Electron density distribution in the meridional plane 110°/290° E in August 2005 at about 18 UT derived from averaged CHAMP data (left panel) and derived from the new plasmasphere model NPSM (right panel).

dependence as being typical for the ionosphere. Both sub-models are fitted independently using the CHAMP data base. Since both sub models are practically decoupled because of quite different scale heights, the electron densities of both parts are simply added. Although being aware that the lower boundary of the plasmasphere is defined by the so-called transition region from a physical point of view we have fixed the lower boundary at 1000 km height in a pragmatic way to keep the algorithm simple. Otherwise one would have to take into account the variability of the transition region that varies around 1000 km height as a result of close coupling with the ionosphere. Considering the limited input data base and the fixed plasmapause position there is still some potential to improve the model output, e.g. by updating the coefficients when using an extended data base and/or by adding a plasmapause model. Nevertheless, we have shown that the presented model approach is able to represent some interesting well known features of the ionosphere/plasmasphere systems. This is the capability to take into account even some features characterizing strong ionospheric coupling resulting in ionospheric anomalies such as the NWA and in conjunction with this also the Weddell Sea and the Ochotsk Sea Anomaly. The model is also able to consider the solar wind induced compression of the plasmasphere. It is evident that the characterisation of this asymmetry will be improved when using data from higher *L*-shells for the determination of coefficients. The model can further be improved and validated by utilizing GNSS measurements on board current and upcoming satellite missions such as GRACE, SWARM or COSMIC 2.

Acknowledgement. The authors are grateful to the international CHAMP team for maintaining the operation and reception of the CHAMP satellite over several years thus establishing a comprehensive data base. The editor thanks Fabien Darrouzet and an anonymous referee for their assistance in evaluating this paper.

References

Belehaki A, Jakowski N, ReinischBW. 2004. Plasmaspheric electron content derived from GPS TEC and digisonde ionograms. *Adv Space Res* **33**: 833–837, DOI:10.1016/j.asr.2003.07.008.

Carpenter DL, Anderson RR. 1992. An ISEE/whistler model of equatorial electron density in the magnetosphere. *J Geophys Res* **97**: 1092–1108, DOI:10.1029/91JA01548.

Chen P, Yao Y. 2015. Research on global plasmaspheric electron content by using LEO occultation and GPS data. *Adv Space Res* **55**: 2248–2255, DOI:10.1016/j.asr.2015.02.004.

Ciraolo L, Spalla P. 1997. Comparison of ionospheric total electron content from the Navy Navigation Satellite System and the GPS. *Radio Sci* **32**: 1071–1080, DOI:10.1029/97RS00425.

Cueto M, Coisson P, Radicella SM, Herraiz M, Ciraolo L, Brunini C. 2007. Topside ionosphere and plasmasphere: use of NeQuick in correlation with Gallagher plasmasphere model. *Adv Space Res* **39**: 739–743, DOI:10.1016/j.asr.2007.01.073.

Daniell RE, Brown LD, Anderson DN, Fox MW, Doherty PH, Decker DT, Sojka JJ, Schunk RW. 1995. Parameterized ionospheric model: a global ionospheric parametrization based on first principles models. *Radio Sci* **30**: 1499–1510, DOI:10.1029/95RS01826.

Darrouzet F, De Keyser J, Pierrard V. (Eds.). 2009. The Earth's plasmasphere: a cluster and IMAGE perspective, Springer, 296 p., ISBN:978-1-4419-1322-7.

Davies K, Fritz RB, Gray TB. 1976. Measurements of columnar electron contents of the ionosphere and plasmasphere. *J Geophys Res* **81**: 2825–2834, DOI:10.1029/JA081i016p02825.

Davies K, Hartmann GK, Leitinger R. 1977. A comparison of several methods of estimating the columnar electron content of the plasmasphere. *J Atmos Terr Phys* **39**: 571–580, DOI:10.1016/0021-9169(77)90066-6.

Denton MH, Bailey GJ, Su YZ, Oyama KI, Abe T. 1999. High altitude observations of electron temperature and a possible north-south asymmetry. *J Atmos Solar-Terr Phys* **61**: 775–788, DOI:10.1016/S1364-6826(99)00036-X.

Förster M, Jakowski N. 1988. The Nighttime Winter Anomaly (NWA) effect in the American sector as a consequence of interhemispheric coupling. *PAGEOPH* **127**: 447–471, DOI:10.1007/BF00879821.

Förster M, Jakowski N. 2000. Geomagnetic storm effects on the topside ionosphere and plasmasphere: a compact tutorial and new results. *Surv Geophys* **21**: 47–87, DOI:10.1023/A:1006775125220.

Gallagher DL, Craven PD, Comfort RH. 1988. An empirical model of the Earth's plasmasphere. *Adv Space Res* **8**: 15–24, DOI:10.1023/A:1006775125220.

Gerzen T, Feltens J, Jakowski N, Galkin I, Denton R, Reinisch BW, Zandbergen R. 2015. Validation of plasmasphere electron density reconstructions derived from data on board CHAMP by IMAGE/RPI data. *Adv Space Res* **55**: 170–183, DOI:10.1016/j.asr.2014.08.005.

He M, Liu L, Wan W, Ning B, Zhao B, Wen J, Yue X, Le H. 2009. A study of the Weddell Sea Anomaly observed by FORMOSAT-3/COSMIC. *JGR* **114**: A12309, DOI:10.1029/2009JA014175.

Heise S, Jakowski N, Wehrenpfennig A, Reigber C, Luehr H. 2002. Sounding of the topside ionosphere/plasmasphere based on GPS measurements from CHAMP: initial results. *Geophys Res Lett* **29**, DOI:10.1029/2002GL014738.

Hoque MM, Jakowski N. 2011. A new global empirical NmF2 model for operational use in radio systems. *Radio Sci* **46**: RS6015, DOI:10.1029/2011RS004807.

Hoque N, Jakowski N. 2012. A new global model for the ionospheric F2 peak height for radio wave propagation. *Ann Geophys* **30**: 787–809, DOI:10.5194/angeo-30-797-2012.

Horvath I, Essex EA. 2003. The Weddell sea anomaly observed with the Topex satellite data. *J Atmos Solar Terr Phys* **65**: 693–706, DOI:10.1016/S1364-6826(03)00083-X.

Huang X, Reinisch BW, Song P, Green JL, Gallagher DL. 2004. Developing an empirical density model of the plasmasphere using IMAGE/RPI observations. *Adv Space Res* **33**: 829–832, DOI:10.1016/j.asr.2003.07.007.

Jakowski N. 2005. Ionospheric GPS radio occultation measurements on board CHAMP. *GPS Solut* **9**: 88–95, DOI:10.1007/s10291-005-0137-7.

Jakowski N, Förster M. 1995 About the nature of the Night-time Winter Anomaly effect (NWA) in the F-region of the ionosphere. *Planet Space Sci* **43**: 603–612, DOI:10.1016/0032-0633(94)00115-8.

Jakowski N, Kugland HG. 1982. Estimation of the electron content of the plasmasphere by means of coherent signals of the ATS-6 satellite received in Neustrelitz. Kosmicheskie Issledovaniya **XX**: 892–1899.

Jakowski N, Bettac HD, Lazo B, Lois L. 1981. Seasonal variations of the columnar electron content of the ionosphere observed in Havana from July 1974 to April 1975. *J Atmos Sol Terr Phys* **43**: 7–11, DOI:10.1016/0021-9169(81)90003-9.

Jakowski N, Förster M, Lazo B, Lois L. 1986. Interhemispheric ionospheric coupling at the American sector during low solar activity, I. Observation. *Gerlands Beitr Geophys* **95**: 219–227.

Jakowski N, Jungstand A, Lois L, Lazo B. 1991. Night-time enhancements of the F2-layer ionization over Havana, *Cuba J Amos Terr Phys* **53**: 1131–1138, DOI:10.1016/0021-9169(91)90062-C.

Jakowski N, Sardon E, Engler E, Jungstand A, Klähn D. 1996. About the use of GPS measurements for ionospheric studies. In: GPS trends in precise terrestrial, airborne, and spaceborne applications. IAG Symposium Nr. 115, (Eds.) Beutler, Hein, Melbourne, Seeber. Heidelberg: Springer-Verlag Berlin, pp. 248–252, DOI:10.1007/978-3-642-80133-4_39.

Jakowski N, Wehrenpfennig A, Heise S, Reigber C, Lühr H, Grunwaldt L, Meehan T. 2002a. GPS radio occultation measurements of the ionosphere from CHAMP: early results. *Geophys Res Lett* **29**, DOI:10.1029/2001GL014364.

Jakowski N, Kutiev IS, Heise S, Wehrenpfennig A. 2002b. A topside ionosphere/plasmasphere model for operational applications. CD-ROM. In: Proceedings of URSI XXVII General Assembly, 17–24 August 2002, Maastricht, paper 2174.

Jakowski N, Wilken V, Mayer C. 2007. Space weather monitoring by GPS measurements on board CHAMP. *Space Weather* **5**: S08006, DOI:10.1029/2006SW000271.

Jakowski N, Hoque MM, Mayer C. 2011a. A new global TEC model for estimating transionospheric radio wave propagation errors. *J Geod* **85**: 965–974. DOI: 10.1007/s00190-011-0455-1.

Jakowski N, Mayer C, Hoque MM, Wilken V. 2011b. TEC models and their use in ionosphere monitoring. *Radio Sci* **46**: RS0D18, DOI:10.1029/2010RS004620.

Jakowski N, Hoque MM, Kriegel M, Patidar V. 2015. The Persistence of the Nighttime Winter Anomaly (NWA) effect during the low solar activity period 2007–2009. *J Geophys Res Space Phys* **120**, DOI:10.1002/2015JA021600.

Kersley L, Klobuchar JA. 1978. Comparison of protonospheric electron content measurements from the American and European

sectors. *Geophys Res Lett* **5**: 123–126, DOI:10.1029/GL005i002p00123.

Kersley L, Klobuchar JA. 1980. Storm associated protonospheric depletion and recovery. *Planet Space Sci* **28**: 453–458, DOI:10.1029/GL005i002p00123.

Klimenko MV, Klimenko VV, Zakharenkova IE, Cherniak IV. 2015. The global morphology of the plasmaspheric electron content during Northern winter 2009 based on GPS/COSMIC observation and GSM TIP model results. *Adv Space Res* **55**: 2077–2085, DOI:10.1016/j.asr.2014.06.027.

Lee HB, Jee G, Kim YH, Shim JS. 2013. Characteristics of global plasmaspheric TEC in comparison with the ionosphere simultaneously observed by Jason-1 satellite. *J Geophys Res* **118**: 935–946, DOI:10.1002/jgra.50130.

Lemaire JF, Gringauz KI. 1998. The Earth's plasmasphere, Cambridge University Press, 350 p., ISBN:0521430917, DOI:10.1017/CBO9780511600098.

Lin CH, Liu CH, Liu JY, Chen CH, Burns AG, Wang W. 2010. Midlatitude summer nighttime anomaly of the ionospheric electron density observed by FORMOSAT-3/COSMIC. *J Geophys Res* **115**: A03308, DOI:10.1029/2009JA014084.

Lunt N, Kersley L, Bishop GJ, Mazzella Jr. AJ. 1999a. The contribution of the protonosphere to GPS total electron content: experimental measurements. *Radio Sci* **34**: 1273–1280, DOI:10.1029/1999RS900016.

Lunt N, Kersley L, Bailey GJ. 1999b. The influence of the protonosphere on GPS observations: model simulations. *Radio Sci* **34**: 725–732, DOI:10.1029/1999RS900002.

Mayer C, Jakowski N. 2007. Comparison of the IRI-2007 Topside Electron Density with CHAMP and COSMIC/Formosat-3 Data. Proc. IRI/COST 296 Workshop, 10–14 July 2007, Prague, Czech Republic.

Mazella Jr AJ. 2009. Plasmasphere effects for GPS TEC measurements in North America. *Radio Sci* **44**: RS5014, DOI:10.1029/2009RS004186.

Mazella Jr. AJ, Holland EA, Andreasen AM, Andreasen CC, Rao GS. 2002. Autonomous estimation of plasmasphere content using GPS measurements. *Radio Sci* **37**: 1092, DOI:10.1029/2001RS002520.

Menk F, Kale Z, Sciffer M, Robinson P, Waters C, Grew R, Clilverd M, Mann I. 2014. Remote sensing the plasmasphere, plasmapause, plumes and other features using ground-based magnetometers. *J Space Weather Space Clim* **4**: A354, DOI:10.1051/swsc/2014030.

Meza A, Natali MP, Fernández LI. 2015. PCA analysis of the nighttime anomaly in far-from-geomagnetic pole regions from VTEC GNSS data. *Earth Planets Space* **67**: 106, DOI:10.1186/s40623-015-0281-4.

Natali MP, Meza A. 2013. The nighttime anomalies using global IGS VTEC maps. *Adv Space Res* **51**: 377–387, DOI:10.1016/j.asr.2012.09.031.

Pierrard V, Voiculescu M. 2011. The 3D model of the plasmasphere coupled to the ionosphere. *Geophys Res Lett* **38**: L12104, DOI:10.1029/2011GL047767.

Pierrard V, Goldstein J, André N, Jordanova VK, Kotova GA, Lemaire JF, Liemohn MW, Matsui H. 2009. Recent progress in physics-based models of the plasmasphere. *Space Sci Rev* **145**: 193–229, DOI:10.1007/s11214-008-9480-7.

Reigber C, Bock R, Förste C, Grunwaldt L, Jakowski N, Lühr H, Schwintzer P, Tilgner C. 1996. CHAMP Phase B – Executive summary. Scientific Technical Report STR96/13, GeoForschungsZentrum, Potsdam.

Reinisch BW, Moldwin MB, Denton RE, Gallagher DL, Matsui H, Pierrard V, Tu J. 2009. Augmented empirical models of plasmaspheric density and electric field using IMAGE and CLUSTER data. *Space Sci Rev* **145**: 231–261, DOI:10.1007/s11214-008-9481-6.

Stolle C, Floberghagen R, Lühr H, Maus S, Knudsen DJ, Alken P, Doornbos E, Hamilton B, Thomson AWP, Visser PN. 2013. Space weather opportunities from the Swarm mission including near real time applications. *Earth Planets Space* **65**: 1375–1383, DOI:10.5047/eps.2013.10.002.

Webb PA, Essex EA. 2004. A global model of the plasmasphere. *J Atmos Solar-Terr Phys* **66**: 1057–1073, DOI:10.1016/j.jastp.2004.04.001.

Yizengaw E, Moldwin MB, Galvan D, Iijima BA, Komjathy A, Mannucci AJ. 2008. Global plasmaspheric TEC and its relative contribution to GPS TEC. *J Atmos Solar-Terr Phys* **70**: 1541–1548, DOI:10.1016/j.jastp.2008.04.022.

Cite this article as: Jakowski N, Hoque MM. 2018. A new electron density model of the plasmasphere for operattepadional applications and services. *J. Space Weather Space Clim.* **8**: A16